A Biomimetic Propulsor for Active Noise Control: Experiments

Promode R. Bandyopadhyay
Mechanical Engineer
Fellow ASME

William P. Krol, Jr.
Mechanical Engineer

Daniel P. Thivierge
Electronics Engineer

William H. Nedderman
Industrial Designer

Naval Undersea Warfare Center
Newport, RI 02841-1708

Mehran Mojarrad
President
Biomimetic Products, Inc.
Cedar Crest, NM 87008-1550

A strategy for the reduction of radiated noise of underwater propulsors has first been developed by means of modeling. It requires a means for blade lift enhancement allowing a lowering of the rotational speed of the propulsor. Laboratory experiments have been carried out with small propulsor models to demonstrate a biomimetic actuator technology for cambering blades actively for lift enhancement. Propulsor blades are constructed partially out of lightweight electroactive polymeric sheets, also known as artificial muscles. The blade motion is digitally controlled and can be complex. Active lift enhancement is demonstrated.

1. Introduction

How to make small underwater moving bodies quieter, is the broad subject of this paper. We start with the assumption that flying and swimming in nature hold the key to new advances in stealth. This may be unsteady hydrodynamic or acoustic mechanisms special to the specie, or an enhancement in the performance of the former leading to gains in the latter. For example, Ellington (1984) an Dickinson *et al*. (1999) have shown that the flight of a fruit fly, which defies conventional steady state aerodynamics, is made possible by the presence of two unsteady rotational aerodynamic mechanisms in additional to the conventional translational mechanism. The present work prepares the groundwork for future consideration of these mechanisms for building new kinds of biologically inspired propulsor blades. So, for a successful application, we need to build a bridge between distilled advances in locomotive biology and appropriately chosen applications. Over the last few years, NUWC has been engaged in such bridge building (Bandyopadhyay *et al.* 1997, 1999 *a, b & c* and 2000 *a & b*).

This paper is concerned with building a case for developing a new approach to the noise reduction of small underwater vehicles. Modeling is carried out in the first section to broadly outline this strategy. A key component of this strategy is then demonstrated experimentally and is described in the next section. A small biomimetic propulsor, with blades made of artificial muscles, is built and demonstrated.

These electroactive muscles have the following appealing features. They are quiet in operation because they require no vibration causing motors, gears or shafting to operate. This feature may be attractive to small underwater bodies where space is a premium.

Finally, these actuators are amenable to digital electronics and programming which make them suitable for active control.

2. Radiated Noise Reduction Strategy

Recent understanding of the mechanism of lift production by fruit fly suggests that they have three sub-mechanisms involved, namely delayed stall, rotational circulation and wake capture (Dickinson *et al*. 1999, Ellington 1984). The former is a translational mechanism, while the latter two involve unsteady hydrodynamics involving a rotation of the blade, which is absent in common man-made lifting surfaces like aircraft wings or blades of rotating fluid machineries like propulsors, helicopter rotors, pumps, compressors and turbines. At NUWC, we are examining the question, how can we incorporate these additional unsteady mechanisms into the blades of the propulsor of a small underwater vehicle? The task is not easy because a blade rotation is needed. However, the availability of certain emerging material technologies suggests that the manufacture of dynamically moving blades might be feasible. The present work is concerned with a demonstration that this is a fruitful path to explore for lift enhancement. The modeling, described below, was then conceived to determine the potential impact of such lift enhancement on stealth.

The details of the modeling of the radiated noise are given in the Appendix. The result is shown in Fig. 1. This shows the reduction in radiated noise due to a reduction in the rotational speed of the propulor (*RPM*). Three sources of noise, other than cavitation, are considered, namely, blade rate tonals due to wake deficits, trailing edge singing and the effect of turbulence ingested from upstream. They are described, approximately by the three power laws, 4, 5 and 6, respectively. Observe that an *RPM* reduction of *10%* can lead to a noise reduction of 3 – 5 *dB*, which is significant. This is the origin of our strategy that an *RPM* reduction should be sought via enhanced blade lift whereby forward speed remains unchanged.

3. Biomimetic Propulsor

A propulsor provides thrust to an underwater vehicle. In this section an experiment on a small propulsor with biomimetic blades incorporating an emerging electro-active material technology is described. The entire experiment is described in a video (Bandyopadhyay *et al*. 2000 *b*).

3.1 Description

A small two-bladed propulsor was constructed and is described below.

3.1.1 Biomimetic Blades

Figure 2 shows the propulsor blades schematically. As shown in Fig. 2(*a*), the blades had a rigid forward part and an artificial muscle was attached to the downstream part. One side of the rigid forepart was flat, and the other had a circular arc. The flat surface of the blade provided a reliable reference for setting the blade pitch during measurements. The muscle was sandwiched between two copper electrodes housed within the trailing end of the rigid part of the blade. The power supply to the electrodes was run through the hollow shaft driving the propulsor shown in Fig. 2 (*c*).

Reinforced type Ionic Polymer Composite membrane artificial muscles, named *MS-417* and *MS-424*, are used. The muscle end is sandwiched between two flat electrodes. When a voltage difference is applied between the electrodes, the muscle becomes charged and deflects (Shahinpoor 1997). It was observed that the muscle deflections were not equal on both sides. One side of the muscle was relatively rough and the other side was smooth. Presumably the charge density on the surfaces was unequal which led to a difference in deflection.

A power supply and digital controller was used to power the muscles. Any one of three voltage pulse forms shown in Fig. 3 could power the muscles. They are bipolar, positively unipolar and negatively unipolar. The figure also shows the pulse forms of current and the bus voltage. The pulse forms, voltage level, frequency and duty cycle could be chosen on a computer monitor via ‘hot keys’.

The various kinds of deflection that could be achieved are shown in Figures 4 and 5. The former shows the deflections for a static blade, while the latter is for a rotating blade. The latter is included as evidence that the muscles remained deflected under the loading of the flow. The pressure difference across the rotating propulsor blade would tend to affect the blade deflection. This may be of the order of what it is for oscillating artificial muscles in static water as shown in the video (Bandyopadhyay *et al*. 2000 *b*). Any reduction of deflection due to pressure difference across the muscle is compensated by higher applied potential difference across the electrodes.

The following deflection options were available. The three kinds of deflections shown are obtained by the three kinds of pulse forms. Furthermore, one could basically purely camber, or purely oscillate or have a combined cambering and oscillation. Cambering was achieved by means of control of the voltage level, while oscillation was achieved by controlling the frequency of pulse form. A low frequency in the range of 1 – 10 *Hz*, roughly, produced an oscillation, while a frequency near 100 *Hz* produced no oscillation. The applied voltage produces a distribution of electric charge on the surface of the muscle. Normally, bubbles form on the muscle surface above 3 *V*. However, a higher frequency generally tended to suppress such bubble formation somewhat beyond 3 *V*. An encapsulated muscle sheet will not produce any bubble. This, therefore, is not a long-term issue.

Figure 4 shows that muscles can be used to increase cambering to increase lift force, or even negatively cambered presumably leading to a thrust reversal. The muscles start moving immediately after they are powered. However, it may take several seconds to reach their steady state deflection.

3.1.2 Experimental Setup

Figure 2 (c) shows the experimental setup schematically. The propulsor is housed in a water filled box of size 295 *mm* x 150 *mm* x 150 *mm*. To avoid degradation of performance of the electrodes and the muscle material, purified de-ionized water was used. This is not a future drawback because the muscles can be encapsulated in deionized water and the electrodes can be made of platinum and made integral to the muscles. These improvements were considered non-essential to the purpose of the present hydrodynamic experiment. The tip to tip diameter of the propulsor is 77 *mm*. The drive shaft is hollow and the muscle power cables run through it to a slip ring located outside the box. The propulsor and drive shaft 'floats'. Before the propulsor was driven, it was slid back upstream and made no contact with the load cell. After the drive starts turning and thrust is produced, the propulsor freely moves downstream and pushes against a load cell situated just outside the box. A '*Nano*' load cell, manufactured by *ATI Inc*. has been used for thrust measurement. The force and moment ranges are12 *N* and 0.12 *Nm*, respectively, and the size of the load cell is 17 *mm* in diameter and 14.5 *mm* in height. This is a six component load cell with monolithic beam construction. Silicon strain gages are built on the beams. The resolution is 0.013 *N* for thrust measurement.

A Personal Computer (PC) is used to operate the load cell controller. Another PC is used for the controller of the muscle power supply. A third main PC is used to collect data from the two PCs and to process and then plot the data.

3.1.2 Base Line Measurements

The measurements of time averaged thrust for varying rotational speed, for an inactive muscle, are shown in Fig. 6. The mean is a *RPM* square trend, as it should be. The Reynolds number based on chord and tip velocity is $1.43x10^4 \leq \mathrm{Re}_c \leq 7.16x10^4$ in the range of $100 \leq RPM \leq 500$. The uncertainty in thrust measurement is large at very low values of *RPM.* Later measurements on turning the muscle on and off are conducted at higher values where the uncertainty should be less. In any case, the present diagnostic involves measurement of changes in thrust between two states, namely when the muscles are deflected or not. In such situations, the absolute accuracy of the thrust values is less important.

To verify, in a different way, that the magnitudes of thrust measurements were reasonable, an order of magnitude calculation was performed to determine the expected thrust. Nondimensionalized $B_P - d$ design curves (relating horsepower to shaft speed) were used for the well-known and documented Series B set of propellers developed by the Netherlands Ship Model Basin at Wageningen. The B2.38 screw was chosen (Todd 1967), as its configuration (number of blades and expanded area ratio) was most similar (but not identical) to the experimental one. The following, standard parameters were used to characterize the propeller:

V_A = speed of advance, meters per second

n = shaft speed, rotations per second

D = maximum propeller diameter, meters

$R = D/2$

J = advance coefficient, $J = \dfrac{V_A}{nD}$

ϕ = pitch angle,

P = pitch for a given radius r, $P = 2\pi r \tan\phi$

s_R = slip ratio, $s_R = 1 - \dfrac{J}{P/D}$

A_e/A_0 = expanded area ratio, $A_e/A_0 = \dfrac{\text{expanded area of all blades}}{\pi R^2}$

Using P/D of the test propeller at the characteristic radius $r = 0.7R$ and assuming s_R to be 25% at design J, it was determined using the design curves that about 0.3 N of thrust would be produced by a well-designed 2-bladed propeller operating at design J and 412 RPM. Its bollard pull (defined as the thrust produced when there is no speed of advance, i.e. $J = 0$, as in the experiment) is a small multiple (say 4) of this value, dependent on the design. The measured bollard pull of 0.45 *N* is therefore well within the expected value for an admittedly non-optimal design. In other words, as per the model, the pull is 4*0.3 *N*, while the measured value is 0.45 *N*. This is a reasonable order of magnitude agreement. The differences between the shape of the Series B blades and the biomimetic blades and the fact that the current experiments were run in a relatively small enclosure would both tend to decrease the expected thrust.

3.2 Results

Thrust measurements were carried out to determine thrust enhancement due to active cambering, that is cambering of the muscles on demand, while the propulsor has been turning at a certain *RPM*. These measurements were carried out by turning the blade muscles off and on to determine the changes. They are shown in Fig. 7 for three values of *RPM*, namely 325, 420 and 520. The flat pressure side of the blades was set to a pitch angle of zero degree to minimize the thrust produced by the propulsor and to maximize the relative effect of the blade cambering. This made detection of the effect of cambering on thrust easier than for a case with a large angle of pitch. The pulse frequency was 1 *Hz*, which led to both cambering and oscillation. Our experience indicates that the electroactive muscle sheets do not deflect equally between one pulse cycle to another and there may be some hysteresis. Thrust response to muscle powering is practically immediate (*O(s)*). There is, roughly, a *15%* increase in thrust when the muscles are cambered.

The significance of the result can be understood in the following manner. A controllable-lift (controllable pitch and camber) propulsor producing *15%* additional thrust compared to a similar conventional propulsor at the same *RPM* can be operated at a *7%* lower *RPM* to produce the same thrust. This could lead to approximately a 1 *dB* reduction in directly-radiated blade tonal noise due to decreased flow velocity over the blade sections.

4. Conclusions

An attempt has been made to develop a strategy for the reduction of noise of small underwater vehicles. Modeling has been carried out which suggests that hydrodynamic strategies for lift enhancement leading to lower rotational speed, is such a route. Unsteady hydrodynamic mechanisms of lift production present in certain swimming and flying animals may be suited for application to propulsor blades. This would require the availability of an active blade cambering technology. Using recently developed electroactive polymeric muscles, the potential of such a digitally amenable technology has been demonstrated on a small laboratory propulsor. The value of active cambering may be in the improvement of propulsor and noise performance in off-design (off-cruise) conditions like maneuvering.

Acknowledgment

This research was funded by the Office of Naval Research (342 Cognitive and Neural S&T Division), Program Manager Dr. Teresa A. McMullen.

References

1. Bandyopadhyay, P. R., Castano, J. M., Nedderman, W. H. & Donnelly, M. J. 2000*a* “Experimental Simulation of Fish-Inspired Unsteady Vortex Dynamics on a Rigid Cylinder,” *ASME Journal of Fluids Engineering*, Vol. 122, No. 2, pp. 219– 238.

2. Bandyopadhyay, P. R. *et al*., 2000*b* “Biomimetics Research at NUWC,” Video (Edited), 14 Mts., Naval Undersea Warfare Center, Newport, RI.

3. Bandyopadhyay, P. R., Singh, S. & Chockalingam, F. 1999*a* “Biologically-Inspired Bodies Under Surface Waves. Part 2: Theoretical Control of Maneuvering“, *ASME Journal of Fluids Engineering*, Vol. 121, No. 2, pp. 479-487.

4. Bandyopadhyay, P. R., Nedderman, W. H. & Dick, J. 1999*b* “Biologically-Inspired Bodies Under Surface Waves. Part 1: Load Measurements“, *ASME Journal of Fluids Engineering*, Vol. 121, No. 2, pp. 469-478.

5. Bandyopadhyay, P. R. 1999c “Emerging Approaches to Flow Control in Hydrodynamics,” Paper CDC99-INV0134, The 38th IEEE Conf. On Decision and Control, Control Systems Society, Dec. 7-10, 1999, Tempe, AZ, Vol. 3 of 5, pp. 2845-2850.

6. Bandyopadhyay, P. R., Castano, J. M., Rice, J. Q., Philips, R. B., Nedderman, W. H. & Macy, W. K. 1997 "Low-speed Maneuvering Hydrodynamics of Fish and Small Underwater Vehicles" *ASME Journal of Fluids Engineering*, V119, pp. 136-144.

5\. Dickinson, M. H., Lehmann, F. & Sane, S. P. 1999 “Wing Rotation and the Aerodynamic Basis of Insect Flight,” *Science*, Vol. 284, 1954-1960.

6. Ellington, C. P. 1984 "The Aerodynamics of Hovering Insect Flight. IV. Aerodynamic mechanisms," *Philosophical Transactions of the Royal Society of London Series B*, Vol. 305, p. 79-113.

7. Shahinpoor, M. 1997 "Ion-Exchange Polymer-Metal Composites As Biomimetic Sensors and Actuators – Artificial Muscles," 10th International Symposium on Unmanned Untethered Submersible Technology, Proceedings of the Special Session on Bio-Engineering Research Related to Autonomous Underwater Vehicles, Sept. 10 & 11, 1997, Organized by Autonomous Undersea Systems Institute, Durham, NH, pp. 62 – 85.

8. F.H. Todd, "Resistance and Propulsion", Principles of Naval Architecture, Chapter 7, p 413, *SNAME*, 1967.

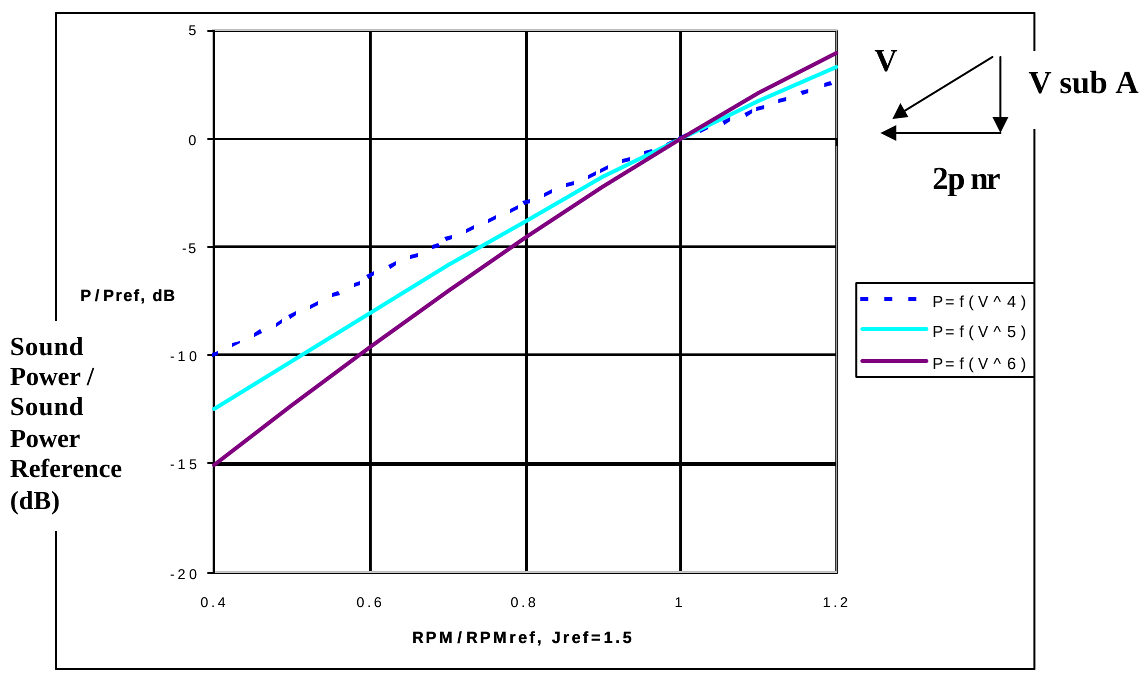

Figure 1. Modeling of the effect of reduction in rotational speed on radiated noise.

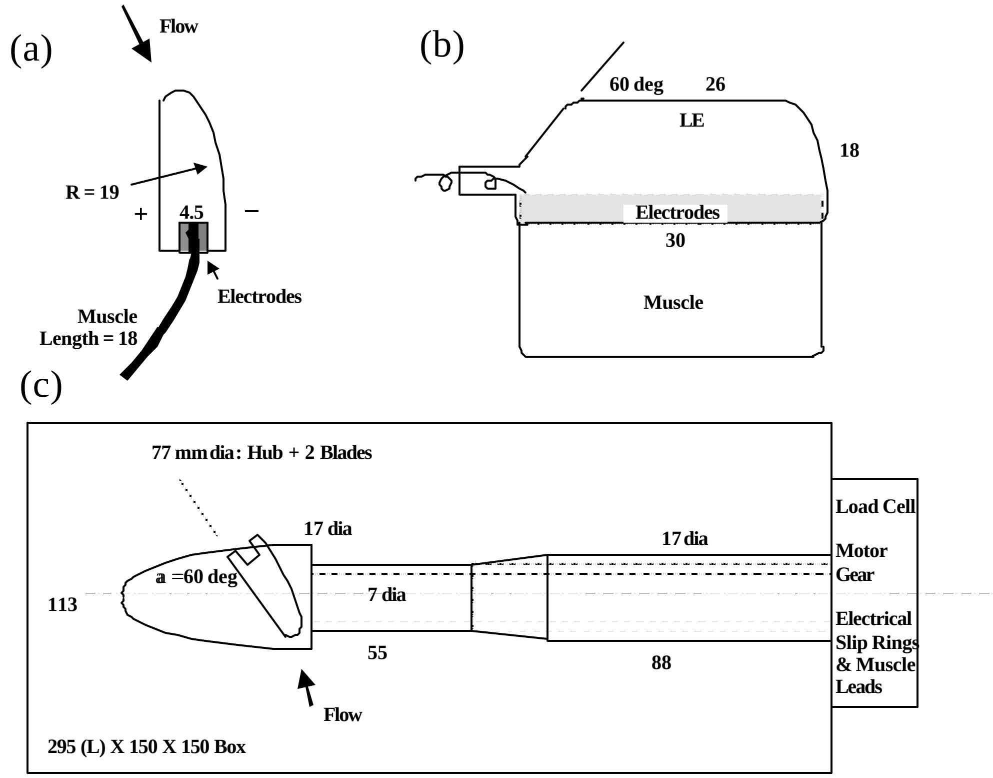

Figure 2. Details of Biomimetic Propulsor: (a) end view of blade with artificial muscle, (b) plan view of blade in (a), and (c) experimental setup of propulsor assembly in water-filled box, with motor drive and load cell.

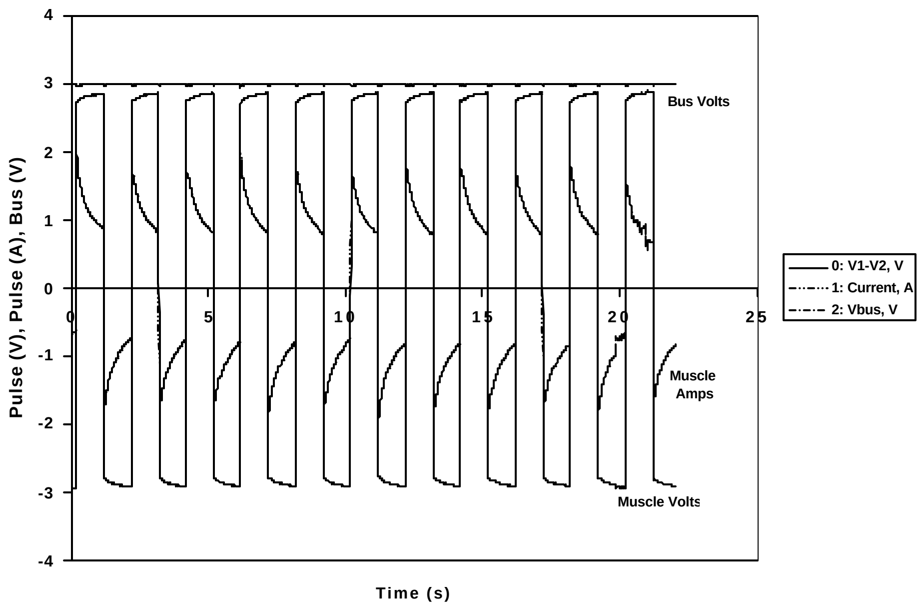

Pulse (V), Pulse (A), Bus (V)
Time (s)
Bus Volts
Muscle Amps
Muscle Volts
0: V1-V2, V
1: Current, A
2: Vbus, V

(a)

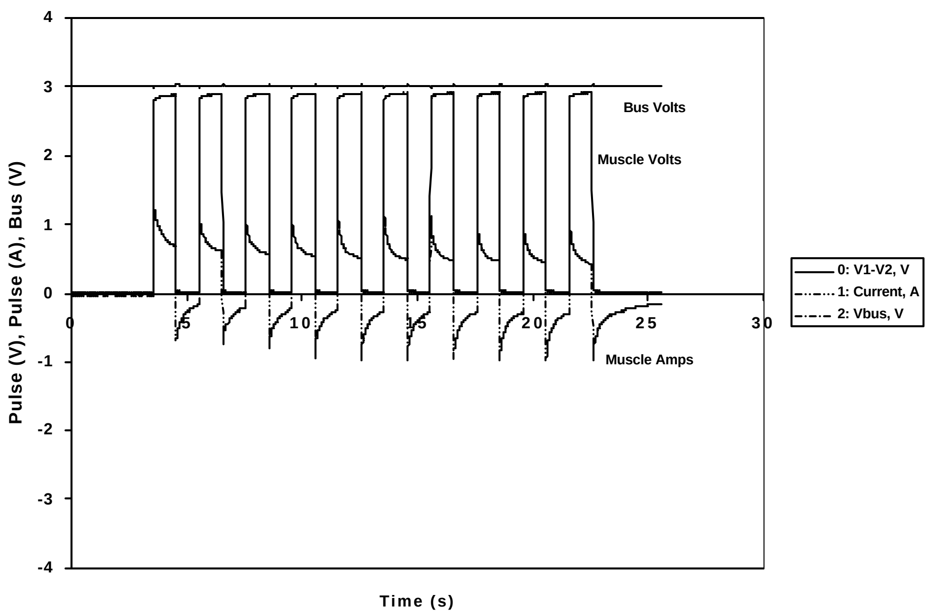

Pulse (V), Pulse (A), Bus (V)
Time (s)
Bus Volts
Muscle Volts
Muscle Amps
0: V1-V2, V
1: Current, A
2: Vbus, V

(b)

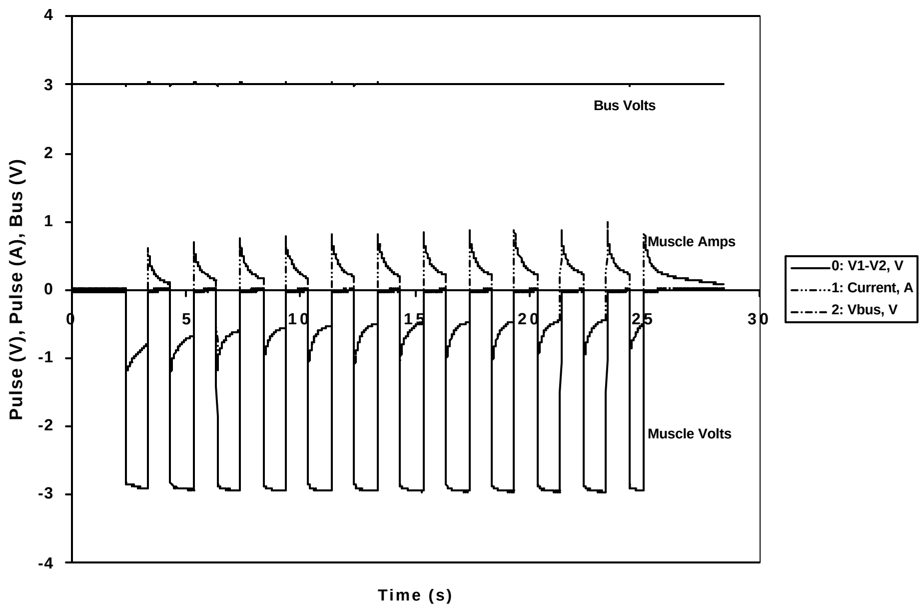

(c)

Figure 3. Pulse forms: (a) Bipolar, (b) Positive Unipolar, and (c) Negative Unipolar. Muscle: *MS-417* with cloth backing; Motion of muscle: (a) Predominantly large amplitude oscillations from flat to large cambering; (b) Predominantly flattens with minor oscillations; (c) Predominantly cambered with minor oscillations; No bubbling; 3 *V*, 1 *Hz*, Duty Cycle *50%*.

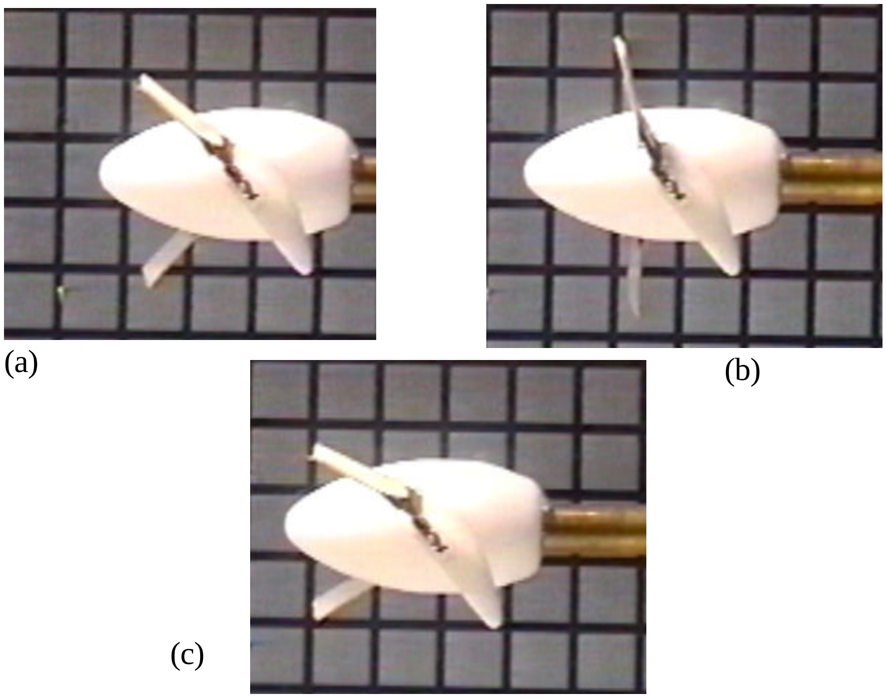

(a) (b) (c)

Figure 4. Cambering of blade muscle. Non-rotating propulsor. Input pulse forms and nature of cambering are as follows. (a) Bipolar: Muscle is Flat, (b) Positive Unipolar: Muscle is Cambered Negatively; Negative Lift – Reversed Thrust, and (c) Negative Unipolar: Muscle is Cambered Positively; Positive Lift – Forward Thrust. Power supply to muscles: 100 *Hz* and 7 *V*; High frequency leads to cambering without oscillation and bubbles; 1 *cm* x 1*cm* Grid.

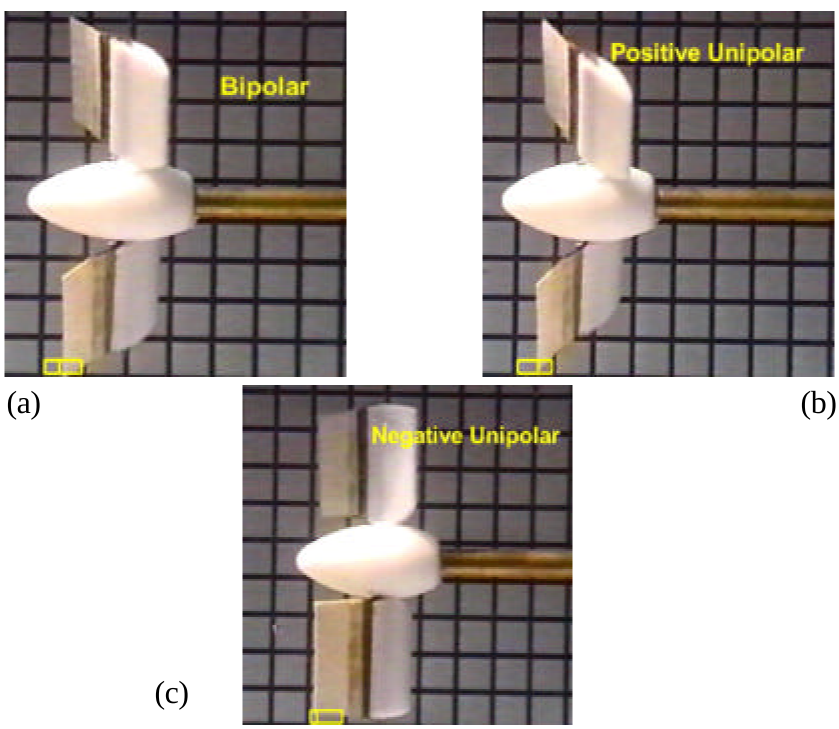

(a) (b) (c)

Figure 5. Rotating propulsor. Stills from video indicating cambering of blade muscles during rotation. Notice trailing edge displacement with respect to marked box during rotation. This displacement indicates that the muscle is staying cambered during rotation. (a) Bipolar; Rotating Propulsor, (b) Positive Unipolar, Rotating Propulsor, and (c) Negative Unipolar, Rotating Propulsor.

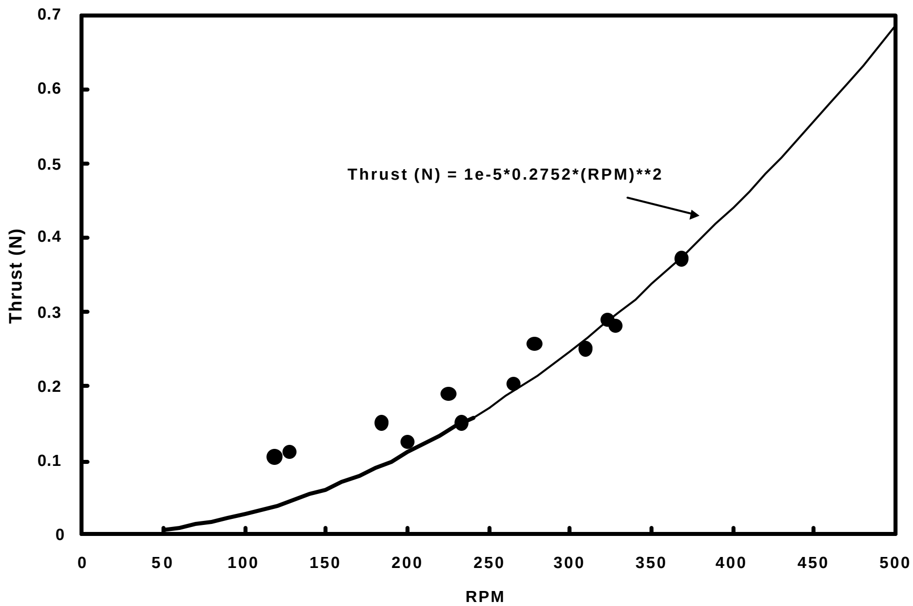

Figure 6. Comparison of measurements of time averaged thrust with *RPM* squared trend. Pitch *73 degrees*; muscles installed but not active. Two bladed propulsor.

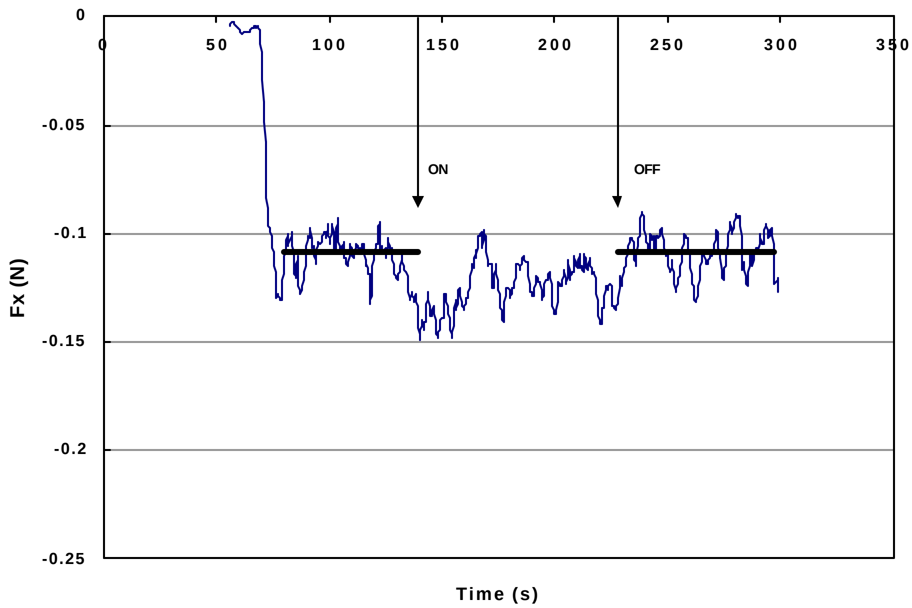
0
-0.05
-0.1
-0.15
-0.2
-0.25
0
50
100
150
200
250
300
350
ON
OFF
Fx (N)
Time (s)

(a)

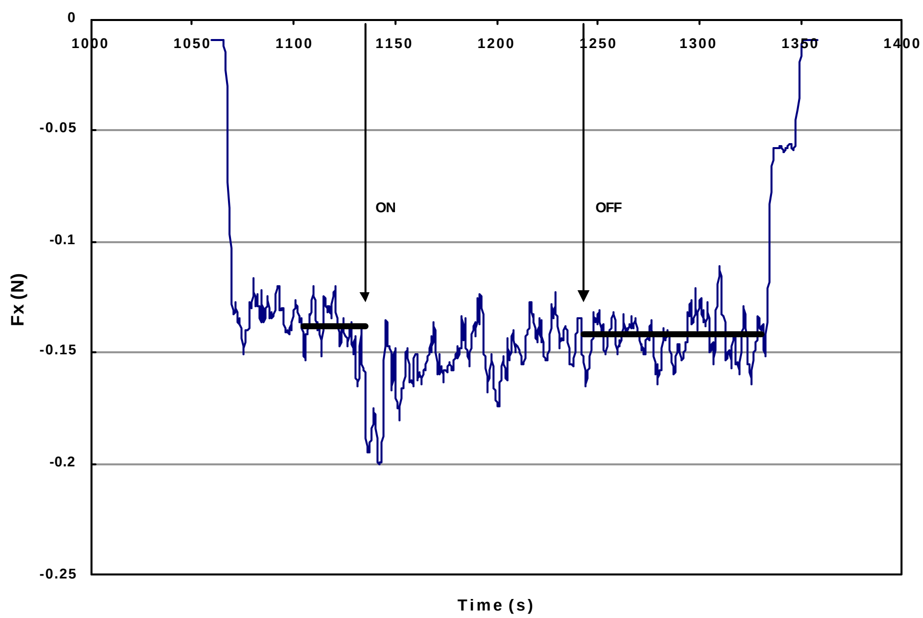
0
-0.05
-0.1
-0.15
-0.2
-0.25
1000
1050
1100
1150
1200
1250
1300
1350
1400
ON
OFF
Fx (N)
Time (s)

(b)

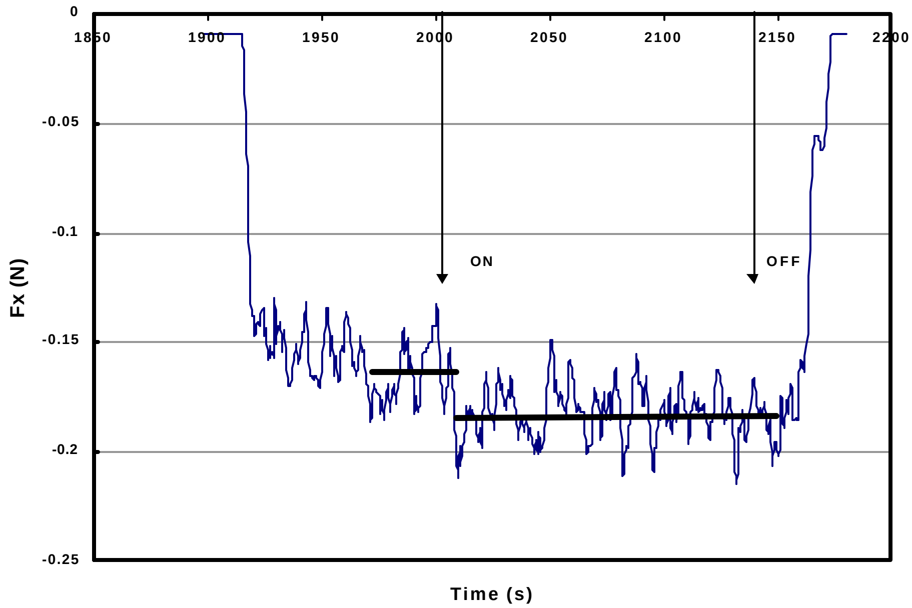

(c)

Figure 7. Comparison of thrust signature during active cambering. Two-bladed propulsor. Values of *RPM* are: (a) 325, (b) 420 and (c) 520. Negative *Fx* indicates positive thrust. Muscle: *MS-417* cloth backing; Power: 3 *V*, 1 *Hz*; No bubbles are produced during these measurements. Pulse: Negative Unipolar producing positive cambering.

Appendix

A1. Mechanics of Propulsor Noise

We wish to examine the dependence of generated noise power on propulsor rotational speed. The following treatment is derived from the one developed in Ross (1987). Throughout, appropriate linearizing assumptions have been made including compactness and the "acoustic assumption" in which physical quantities may be expressed as sums of steady-state and fluctuating values. That is, for the general quantity *A*, position coordinates *x*, *y*, *z*, time *t*, and period *T*,

$$A(x,y,z,t) = A_0(x,y,z) + A'(x,y,z,t) \qquad (1.)$$

$$A_0 = \frac{1}{T}\int_0^T A\,dt \qquad (2.)$$

A governing equation for sound generation based on Lighthill (1952) can be expressed in tensor notation as

$$\nabla^2 p' - \frac{1}{c_0^{\,2}}\ddot{p}' = -\dot{q}' + \nabla\cdot\vec{f}' - \frac{\partial \tau'_{ij}}{\partial x_i \partial x_j} \qquad (3.)$$

where p', q', $\vec{f}'$, and τ'_{ij} are the fluctuating components of pressure, mass, force, and the turbulent stress tensor respectively, c_0 is sound speed, and dots represent partial derivatives with respect to time. The three terms of the right-hand side above represent noise due to 1) fluctuating volumes, 2) fluctuating forces, and 3) turbulence, respectively.

A1.1 Fluctuating Volumes

The example of noise due to fluctuating volumes relevant to propulsors is from cavitation. It can be shown that the sound power due to this mechanism is proportional to the fourth power of blade tip speed. It is assumed that normally torpedo and submarine propulsors will be operated in regimes where cavitation does not occur; therefore, fluctuating volume noise will not be considered further.

A1.2 Fluctuating Forces

The operation of a propulsor in a circumferentially non-uniform wake produces fluctuating thrust and side forces. This causes direct acoustic dipole radiation into the surrounding fluid independent of any resultant structural vibration. Usually, the most significant consequence of any propulsor blade vibration is transmission to attached structures and subsequent re-radiation. The modeling of structural vibrations is complex and beyond the current scope; the focus here will remain on direct radiation. Fortunately, reduction of the fluctuating forces causing directly-radiated sound also attenuates the structural forcing functions and the resultant indirect sound radiation.

The following analysis is for thrust but can be applied to other force components. Circumferential variation in inflow causes oscillations in thrust at multiples of the blade frequency, *f*:

$$f = mBn \qquad (4.)$$

where *m* is the order of the harmonic, *B* is the number of blades, and *n* is the speed in rotations per second. The non-dimensionalized unsteady thrust $\tilde{C}_{T_m}$ for the *m*-th harmonic is expressed as

$$\tilde{C}_{T_m} = \frac{\tilde{T}_m}{\rho_0 n^2 D^4} \qquad (5.)$$

where $\tilde{T}_m$ is the fluctuating component of thrust, ρ_0 is the steady-state fluid density, and D is the diameter. For wave lengths large compared to the body, that is, $kD < 1$ where

$$kD = \frac{2\pi mBnD}{c_0} \quad (6.)$$

the acoustic power W_{ac} can be derived as

$$W_{ac} = \frac{m^2B^2}{3c_0^{\,3}}\,\rho_0 n^6 D^8 \left(\tilde{C}_{T_m}\right)^2 \quad (7.)$$

Acoustic power is therefore proportional to the sixth power of blade tip speed, $n\pi D$. Empirical evidence (the phenomenon of “trailing edge singing” of the blades of some tactical-scale vehicle propulsors) along with theory (Lawson (1970)) have shown that for $kD > 2$, acoustic power is actually proportional to the fifth power of blade tip speed.

A.3 Turbulence

The fluctuating component of the turbulent stress tensor, τ'_{ij}, is given by

$$\tau'_{ij} = \left(\rho v_i v_j\right)' + \left(p'_{ij} - p'\delta_{ij}\right) + \left(p' - c_0^{\,2}\rho'\right)\delta_{ij} \quad (8.)$$

where ρ is density, v_i is the i-th component of particle velocity, p_{ij} is a pressure stress tensor, and δ_{ij} is the Kronecker Delta. The terms in the right-hand side represent fluctuating shear stresses associated with, respectively, 1) turbulent fluid motions, 2) viscous stresses, and 3) heat conduction and/or nonlinearity. Only the first is of significance in liquid flows and can be approximated to first order by

$$\tau'_{ij} = 2\,\rho_0 U_0 u'_i \quad (9.)$$

where U_0 is the flow speed and u'_i is the *i*-th component of the fluctuating hydrodynamic velocity. This leads to an expression for the sound generated by turbulence assuming a source region small compared to the sound wavelength:

$$p' = \frac{\rho_0 U_0}{2\pi r}\frac{\partial^2}{\partial x_i \partial x_j}\int_V u'_i \, dV \quad (10.)$$

where V is the source volume. This sound is quadrupole in nature; its power is proportional to the sixth power of the flow speed.

Appendix References

Lawson, M. V., 1970, Theoretical analysis of compressor noise, Journal of the Acoustical Society of America, 47 p. 371-385.

Lighthill, M.J., 1952, “On sound generated aerodynamically: 1. General theory”, Proceedings of the Royal Society, A211, p.1107.

Ross, D, 1987, *Mechanics of Underwater Noise*, Peninsula Publishing, Los Altos, California.